mass 40,000–41,000 (40–41K) had been ADP-ribosylated, so that *in vitro* incorporation by PTX of [^{32}P]ADP-ribose into the protein was attenuated by 79±9% ($n=5$; $P<0.01$). These results strongly indicate that endothelin-1 induces the electrophysiological responses through a PTX-sensitive GTP-binding protein, probably G_i or G_o.

Endothelins are released in various stressful conditions such as cardiac infarction and congestive heart failure[6,24], where sympathetic tone is extensively elevated. Therefore, interaction of endothelins with sympathetic neurotransmitters[25] may play a very important role in both physiological and pathophysiological states. Using β-adrenoceptor stimulation as an example of such conditions, we found that endothelin-1, through the ET_A receptors, exerts a negative modulatory action by interacting with certain ion channels. Our results provide the first direct evidence that the ET_A receptors mediate hyperpolarization and shortening of the action potential duration by inhibiting I_{Ca} and stimulating $I_{K(ACh)}$ in adult mammalian heart under physiological conditions. The effects are coupled to a PTX-sensitive GTP-binding protein and the inhibition of cAMP accumulation. These ET_A-receptor-mediated electrophysiological actions of endothelin-1 may give important insights into our understanding of the physiological and pathophysiological regulation of heart functions. □

Received 28 March; accepted 22 June 1994.

1. Ono, K., Delay, M., Nakajima, T., Irisawa, H. & Giles, W. *Nature* **340,** 721–724 (1989).
2. Reuter, H. *A. Rev. Physiol.* **41,** 413–424 (1979).
3. Yanagisawa, M. *et al. Nature* **332,** 411–415 (1988).
4. Ishikawa, T., Yanagisawa, M., Kimura, S., Goto, K. & Masaki, T. *Am. J. Physiol.* **255,** H970–H973 (1988).
5. Ishikawa, T., Yanagisawa, M., Kimura, S., Goto, K. & Masaki, T. *Pflügers Arch. ges. Physiol.* **413,** 108–110 (1988).
6. Masaki, T., Yanagisawa, M. & Goto, K. *Med. Res. Rev.* **12,** 391–421 (1992).
7. Aramori, I. & Nakanishi, S. *J. biol. Chem.* **267,** 12468–12474 (1992).
8. Ihara, M. *et al. Life Sci.* **50,** 247–255 (1992).
9. Arai, H., Hori, S., Aramori, I., Ohkubo, H. & Nakanishi, S. *Nature* **348,** 730–732 (1990).
10. Sakamoto, A. *et al. J. biol. Chem.* **268,** 8547–8553 (1993).
11. Sakurai, T. *et al. Nature* **348,** 732–735 (1990).
12. Franco-Cereceda, A., Matran, R., Lou, Y.-P. & Lundberg, J. M. *Acta physiol. scand.* **138,** 539–547 (1990).
13. Tohse, N., Hattori, Y., Nakaya, H., Endou, M. & Kanno, M. *Br. J. Pharmac.* **99,** 437–438 (1990).
14. Hartzell, H. C. & Simmons, M. A. *J. Physiol., Lond.* **389,** 411–422 (1987).
15. Pfaffinger, P. J., Martin, J. M., Hunter, D. D., Nathanson, N. M. & Hille, B. *Nature* **317,** 536–538 (1985).
16. Kim, D. *Circ. Res.* **69,** 250–255 (1991).
17. Sakamoto, A. *et al. Biochem. biophys. Res. Commun.* **178,** 656–663 (1991).
18. Inoue, A. *et al. Proc. natn. Acad. Sci. U.S.A.* **86,** 2863–2867 (1989).
19. Tanaka, T. *et al. Molec. Pharmac.* **45,** 724–730 (1994).
20. Ishikawa, T. *et al. Circ. Res.* **69,** 918–926 (1991).
21. Hori, S., Komatsu, Y., Shigemoto, R., Mizuno, N. & Nakanishi, S. *Endocrinology* **130,** 1885–1895 (1992).
22. Hilal-Dandan, R., Urasawa, K. & Brunton, L. L. *J. biol. Chem.* **267,** 10620–10624 (1992).
23. Vogelsang, M., Broede-Sitz, A., Schäfer, E., Zerkowski, H.-R. & Brodde, O.-E. *J. cardiovasc. Pharmac.* **23,** 344–347 (1994).
24. Wennmalm, A., Benthin, G., Karwatowska-Prokopczuk, E., Lundberg, J. & Petersson, A.-S. *J. Physiol., Lond.* **435,** 163–173 (1991).
25. Reid, J. J., Lieu, A. T. & Rand, M. J. *Eur. J. Pharmac.* **194,** 173–181 (1991).
26. Hamill, O. P., Marty, A., Neher, E., Sakmann, B. & Sigworth, F. J. *Pflügers Arch. ges. Physiol.* **391,** 85–100 (1981).
27. Ono, K. & Giles, W. R. *J. Physiol., Lond.* **436,** 195–217 (1991).

ACKNOWLEDGEMENTS. We thank W. R. Giles (Departments of Medical Physiology and Medicine, University of Calgary, Canada) for his helpful discussion and M. Ihara and M. Yano of Banyu Pharmaceutical Co. Ltd, Japan and Y. Matsuda of Kyowa Hakko Kogyo Co., Japan for kindly providing BQ123 and RES-701-1, respectively. This work was supported in part by the Alberta Heritage Foundation for Medical Research, Canada, and Research Grant for Encouragement of Young Researchers, Ministry of Science and Education, Japan. K.O. thanks Nissan Science Foundation, Japan for financial support.

Mice with targeted disruptions in the paralogous genes *hoxa-3* and *hoxd-3* reveal synergistic interactions

Brian G. Condie & Mario R. Capecchi*

Howard Hughes Medical Institute, Department of Human Genetics, University of Utah School of Medicine, Salt Lake City, Utah 84112, USA

THE *Hox* genes encode transcription factors which mediate the formation of the mammalian body plan along the anteroposterior and appendicular axes[1–15]. Paralogous *Hox* genes within the separate linkage groups are closely related with respect to DNA sequence and expression[16,17], suggesting that they could have at least partially redundant functions. We showed previously that mice homozygous for independent targeted disruptions in the paralogous genes *hoxa-3* and *hoxd-3* had no defects in common[1,8]. But our current analysis of double mutants has revealed strong, dosage-dependent interactions between these genes. We report here that in *hoxd-3*$^-$ homozygotes the first cervical vertebra, the atlas, is homeotically transformed to the adjacent anterior structure. Unexpectedly, in double mutants, rather than observing a more extensive homeotic transformation, the entire atlas is deleted. These observations are interpreted in terms of a model in which these *Hox* genes differentially regulate the proliferation rates of the appropriate sets of precursor cells.

The absence of overlapping abnormalities in *hoxa-3*$^-$ and *hoxd-3*$^-$ mutant mice does not imply that these two genes do not interact. To investigate such interactions, we generated mice that are simultaneously mutant for both genes. Because *hoxa-3*$^-$ and *hoxd-3*$^-$ homozygotes usually die shortly after birth (*hoxa-3*$^-$/*hoxa-3*$^-$ mice from cardiovascular dysfunction and *hoxd-3*$^-$/*hoxd-3*$^-$ mice from apparent accidental cervical dislocation as a result of a destabilized craniocervical joint), double homozygotes were generated by intercrossing compound heterozygotes. From these intercrosses, 284 full-term progeny were produced. Of these, 14 were double homozygotes, very close to the expected frequency of 1/16, indicating that such mice do not die during embryogenesis.

Figure 1 shows lateral views of skeleton preparations of wild-type mice, *hoxa-3*$^-$ homozygotes, *hoxd-3*$^-$ homozygotes and double mutants. The craniocervical joint of *hoxa-3*$^-$ homozygotes is indistinguishable from that of wild-type animals (compare Fig. 1*a* and *b*). The *hoxd-3* mutation alone results in a remodelling of the bones in the craniocervical joint. In these mice, the anterior arch of the atlas forms an extension of the basioccipital bone, the atlas lateral masses are remodelled to resemble and are often fused to the exoccipitals, the axis is remodelled to resemble the atlas, the dens and the superior facets of the axis are deleted and the lateral foramina normally associated with the atlas are now attached to the axis (Fig. 1*c* and ref. 8). The double mutant mouse, however, shows a more severe phenotype. The entire atlas has been deleted, and only a small piece of cartilage remains in its place (Fig. 1*d*). This deletion of

FIG. 2 The deletion of the atlas depends on the dosage of *Hoxa-3* ► mutant alleles in the *hoxd-3*$^-$ homozygote. Lateral views of cleared skeleton preparations of newborn mice. *a*, The craniocervical region in a wild-type newborn (a3+/+; d3+/+). The atlas (at) and axis (ax) are indicated. The arrow indicates the ossification centre in the anterior arch of the atlas. *b*, Same view of a *hoxd-3* heterozygote (a3+/+; d3+/−). *c*, The atlas is further altered in this compound heterozygote (a3+/−; d3+/−). The ossification centre in the anterior arch of the atlas has failed to form (arrow). *d*, A *hoxd-3* homozygote (a3+/+; d3−/−) with a nearly complete homeotic transformation of the atlas. This is an example of the most extreme *hoxd-3* phenotype. *e*, Compared with the *hoxd-3*$^-$ homozygote, the atlas is more severely affected in the (*hoxa-3*$^+$/*hoxa-3*$^-$; *hoxd-3*$^-$/*hoxd-3*$^-$) mouse. *f*, A double-mutant newborn (a3−/−; d3−/−). The atlas is deleted and cartilaginous fusions between the neural arches of the axis and other cervical vertebrae are indicated (arrow). Scale bar, 1.0 mm.

* To whom correspondence should be addressed.

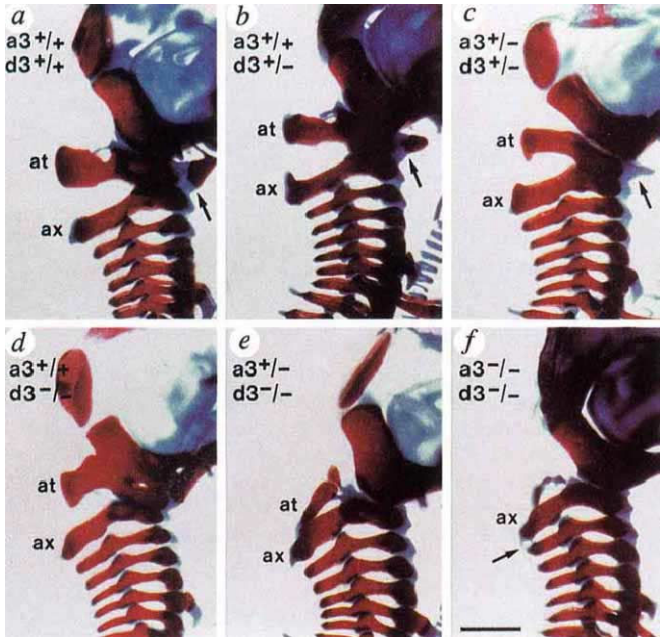

FIG. 1 Additional skeletal defects in (*hoxa-3*$^{-}$/*hoxa-3*$^{-}$; *hoxd-3*$^{-}$/*hoxd-3*$^{-}$) mice. Lateral views of cleared skeleton preparations of newborn mice. *a*, A wild-type (a3+/+; d3+/+) newborn, the first cervical vertebra or atlas (at) and the second cervical vertebra or axis (ax) are labelled. *b*, A *Hoxa-3* homozygote (a3−/−; d3+/+). *c*, A *Hoxd-3* homozygote (a3+/+; d3−/−) displaying the characteristic homeotic transformation of the atlas (at). *d*, A *hoxa-3*, *hoxd-3* double homozygote (a3−/−; d3−/−) showing the complete absence of the atlas and remodelling of the axis (ax). Scale bar, 1 mm.
METHODS. Newborn skeleton preparations were made as described[21].

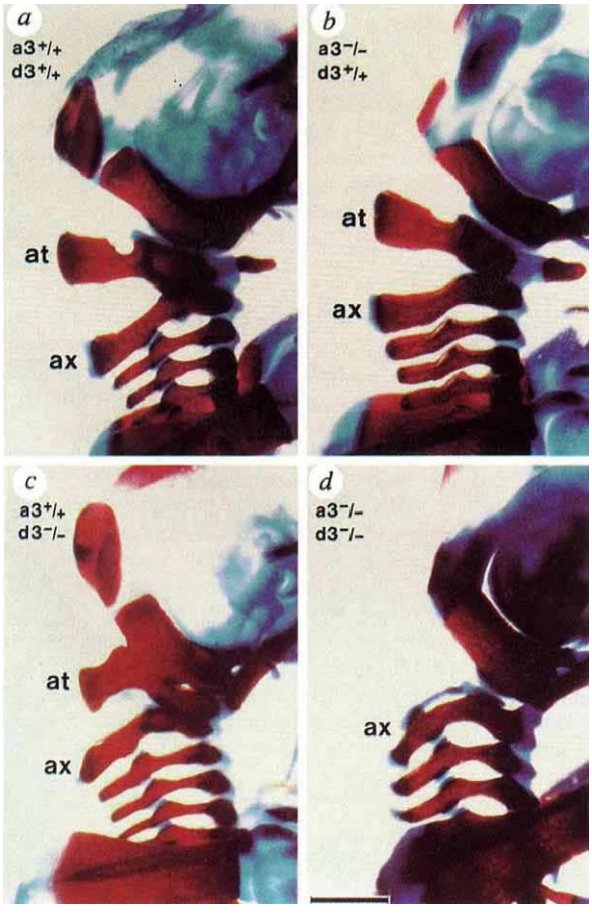

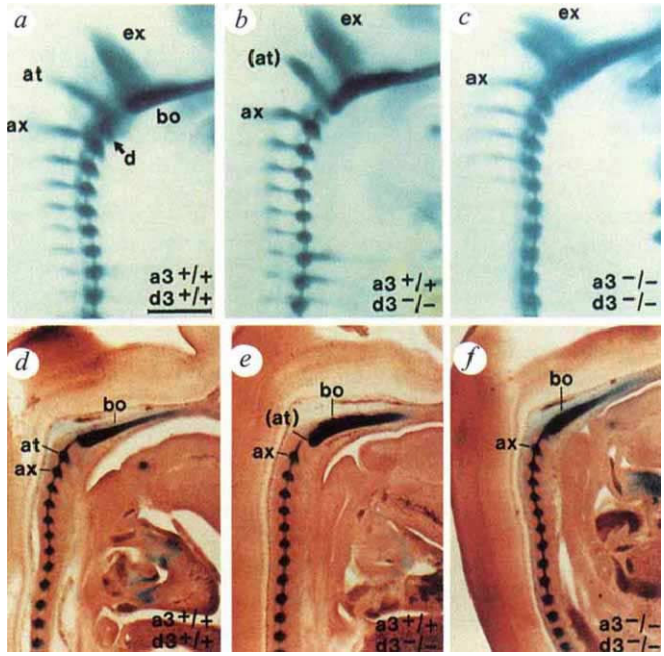

FIG. 3 The pattern of the cartilage condensations in E13 embryos. *a*–*c*, Lateral views of cleared preparations of mouse embryos. *a*, A wild-type embryo (a3+/+; d3+/+). The cartilage anlagen of the basioccipital (bo), exoccipital (ex), atlas (at), axis (ax) and dens (d) are indicated. *b*, A *hoxd-3* homozygous embryo (a3+/+; d3−/−). *c*, A double-mutant embryo (a3−/−; d3−/−). The atlas is deleted and the cartilage anlage of the axis is indicated. *d*–*f*, Midsagittal thick sections (100 μm) of the embryos pictured in *a*–*c*. *d*, The wild-type embryo (a3+/+; d3+/+), the cartilage anlagen for the basioccipital (bo), atlas (at) and axis (ax) are indicated. *e*, The *hoxd-3* homozygote (a3+/+; d3−/−). *f*, The double-mutant embryo (a3−/−; d3−/−). The assignment of the cervical vertebrae anlagen in wild-type and mutant mice was confirmed by counting rostrally from the first thoracic vertebra anlage. Scale bar, 0.5 mm.
METHODS. Embryos were collected on embryonic day 13 (morning of the plug is 0.5 days), stained with Alcian blue and cleared as described[22]. Stained embryos were removed from benzyl benzoate/benzyl alcohol into methanol, rehydrated in PBS, embedded in 3% agarose and sectioned at 100 μm on a vibratome. Sections were dried onto gelatin subbed slides, counterstained with nuclear Fast red and mounted in 90% glycerol/PBS.

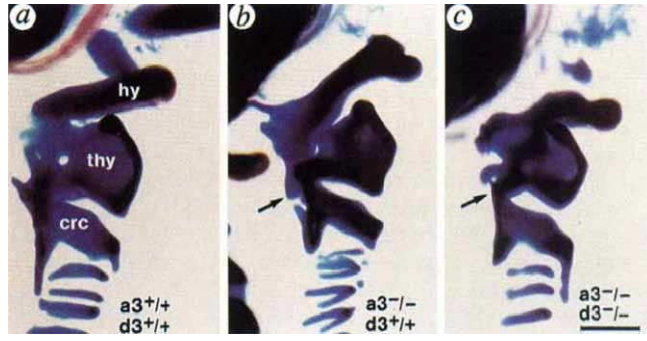

FIG. 4 The *Hoxa-3*$^{-}$ defects are more severe in (*hoxa-3*$^{-}$/*hoxa-3*$^{-}$; *hoxd-3*$^{-}$/*hoxd-3*$^{-}$) mice. Lateral views of skeleton preparations of newborn mice. *a*, The laryngeal cartilages in a wild-type (a3+/+; d3+/+) newborn mouse. The hyoid bone (hy), thyroid (thy) and cricoid (crc) cartilages are indicated. *b*, The laryngeal cartilages of a *hoxa-3* (a3−/−; d3+/+) mutant. The arrow indicates the inferior horn of the thyroid cartilage. *c*, Lateral view of a double homozygote (a3−/−; d3−/−). Remodelling has changed the appearance of the hyoid and thyroid cartilages. The dorsal side of the thyroid cartilage (left side) is altered because of the deletion of cartilage and the inferior horn of the thyroid cartilage is missing (arrow). Scale bar, 0.5 mm.

the atlas was observed in all six of the double mutant skeletons examined. The axis has also been remodelled to appear more like a 'generic' cervical vertebra.

We reported previously[8] that at low penetrance, mice heterozygous for the *hoxd-3*$^-$ mutation have mild abnormalities in the craniocervical joint (Fig. 2*b*). The anterior arch of the atlas is reduced in size and has small, unilateral fusions with the basioccipital bone. These results suggested that the dosage of the *hoxd-3* protein is an important factor in determining the severity of the abnormalities, and raised the possibility that the interactions between *hoxa-3* and *hoxd-3* might also be quantitative (that is, dosage-dependent). Figure 2 shows that the severity of the craniocervical joint abnormality indeed increases as the number of wild-type copies of *hoxa-3* and *hoxd-3*$^-$ decreases. Compound heterozygotes (*hoxa-3*$^-$/*hoxa-3*$^+$; *hoxd-3*$^-$/*hoxd-3*$^+$) show a more severe mutant phenotype at higher penetrance (45% versus 15%) than mice heterozygous for the *hoxd-3*$^-$ mutation alone (compare Fig. 2*b* and *c*). The anterior arch of the atlas is more reduced and the atlas lateral masses are more extensively remodelled than in *hoxd-3*$^-$/*hoxd-3*$^+$ mice; also note the absence of the lateral foramina. In addition, whereas the *hoxd-3*$^-$ heterozygotes always have a dens, in the most strongly affected compound heterozygotes the dens is deleted. Furthermore, (*hoxa-3*$^-$/*hoxa-3*$^+$; *hoxd-3*$^-$/*hoxd-3*$^-$) mice have a phenotype intermediate between that of the (*hoxa-3*$^+$/*hoxa-3*$^+$; *hoxd-3*$^-$/*hoxd-3*$^-$) and (*hoxa-3*$^-$/*hoxa-3*$^-$; *hoxd-3*$^-$/*hoxd-3*$^-$) mice (Fig. 2*d–f*). Parts of the atlas are progressively deleted as one and then two wild-type copies of *hoxa-3* are removed from the *hoxd-3*$^-$ homozygous mutant background.

The bones of the vertebral column are formed by the endochondral pathway in which a cartilaginous prototype is laid down before bone formation. The effect of the *hoxd-3*$^-$ and *hoxa-3*$^-$ mutations can be seen as the precartilaginous condensations are formed. Figure 3*a* shows a lateral view of an E13 wild-type embryo stained to reveal the cartilage anlagen. Figure 3*d* shows a sagittal section of the same embryo counterstained with nuclear fast red. The precartilaginous condensations that give rise to the basioccipital, the exoccipitals, the atlas, the axis and the dens are evident. In the *hoxd-3*$^-$ homozygotes (Fig. 3*b*, *e*), the cartilage anlage that would form the atlas is shifted towards the base of the skull and fused along its ventral aspects with the basioccipital anlage (Fig. 3*e*). The shape of the axis anlage has changed to resemble more closely the atlas anlage and the dens anlage is severely reduced or absent. In the double mutant (Fig. 3*c*, *f*), only a vestige of the atlas anlage remains ventral to the notocord. Thus, the change of the *hoxd-3* phenotype in the double mutants is evident at this embryonic stage.

Figure 4 shows that the *hoxa-3* mutant phenotype is similarly exacerbated in mice also mutant for *hoxd-3*. In *hoxa-3* mutants, the lesser horns of the hyoid bone are reduced or missing and the greater horn of the hyoid is fused with the superior horn of the thyroid cartilage (Fig. 4*b*). In *hoxd-3*$^-$ homozygotes these elements are not affected[8]. In the double mutant, the hyoid is reduced in size and fuses closer to the body of the thyroid cartilage (Fig. 4*c*). In addition to these changes, cartilage is missing dorsally, creating gaps and holes in the lamina of the thyroid cartilage. Also, the inferior horns of the thyroid cartilage are deleted. These deletions reduce the size of the thyroid cartilage and give it a very different appearance from those of the wild-type and *hoxa-3*$^-$ homozygous mutants (Fig. 4*a–c*). The exacerbation of the *hoxa-3* phenotype by the *hoxd-3*$^-$ mutation is also dosage-dependent. For example, although neither *hoxa-3* and *hoxd-3* heterozygotes nor *hoxd-3* homozygotes show defects in the hyoid/thyroid cartilages, compound heterozygotes (*hoxa-3*$^-$/*hoxa-3*$^+$: *hoxd-3*$^-$/*hoxd-3*$^+$) exhibit fusions between the hyoid and thyroid cartilages (data not shown).

Not all of the *hoxa-3*$^-$ phenotypes are exacerbated by the *hoxd-3*$^-$ mutation. For example, the defects of the heart and its great vessels are the same in *hoxa-3*$^-$ homozygotes and in the double mutants. Also, the extent of truncation of the soft palate and the reduction in the thyroid and submaxillary glands in *hoxa-3*$^-$/*hoxa-3*$^-$ and (*hoxa-3*$^-$/*hoxa-3*$^-$; *hoxd-3*$^-$/*hoxd-3*$^-$) mice appear to be the same. In contrast some *hoxa-3*$^-$ homozygotes have remnants of a thymus, whereas all double mutants are athymic. Also, the phenotype of the epiglottis in double mutants is more severe than in *hoxa-3*$^-$ homozygotes.

Analysis of mice with mutations in both *hoxa-3* and *hoxd-3* has revealed strong genetic interactions between these two genes. The double-mutant mice have more severe abnormalities than predicted from the sum of the individual mutant phenotypes. In the double mutants the entire atlas was deleted rather than being more extensively transformed into the adjacent anterior bones. The extent of deletion of the atlas in *hoxd-3*$^-$/*hoxd-3*$^-$ mice increased progressively with the loss of one and then two copies of the wild-type *hoxa-3* gene. The deletion of the atlas precursors could be detected in E13 embryos, indicating that the defects seen in the newborn animals reflect changes in the early patterning of the cartilage anlagen for these bones.

To explain the observation that in *hoxd-3*$^-$/*hoxd-3*$^-$ mice parts of the atlas and axis were homeotically transformed to resemble more anterior structures, whereas other parts were deleted, we suggested a model whereby the *hoxd-3* product differentially regulates the rate of proliferation of precursor cells[8]. Our finding that the entire atlas is deleted in the double mutant lends support to this model. In mice carrying both mutations, we propose that all of the precursor cells responsible for the formation of the atlas fail to proliferate, and thus cannot form the atlas.

In the context of this model, note that *hoxb-8* is transcriptionally activated in mouse myeloid leukaemia WEH1-3B cells, and that transfection of this gene into NIH-3T3 cells produces fibrosarcomas in nude mice[18]. Thus, at least some *Hox* genes can function as oncogenes, and are implicated in controlling cell proliferation. Similarly, the sets of limb defects resulting from targeted disruption of *hoxa-11, hoxd-11* and *hoxd-13* are more readily interpreted in terms of localized perturbations of the growth of cells, than in terms of specification of digit identity[10,11,15]. Furthermore, the metameric hindbrain pattern is perturbed in *hoxa-1*$^-$/*hoxa-1*$^-$ mice[6,7,19]. In these mutants, rhombomere 5 is missing and the integrity of rhombomeres 4–7 is compromised. These results are also readily interpreted in terms of a role for *hoxa-1* in mediating cell proliferation within the neural tube. Postulating roles for *Hox* genes in regulating proliferation of precursor cells is conceptually quite different from postulating a role in the specification of cell identity. The former may be less complex than the latter and might not require a complex '*Hox*-code'[20]. However, these roles are not mutually exclusive.

Alternatively, the deletion of the atlas in the double mutants could be explained by increased programmed cell death. However, careful histological examination of E9.0 to E13.0 embryos has not revealed an excess of pycnotic cells in the double mutants relative to normal controls during the formation of the craniocervical joint anlage.

It is curious that mice homozygous for either the *hoxa-3*$^-$ or *hoxd-3*$^-$ mutation show no overlap in phenotype. However, the double-mutant phenotype demonstrates that these two gene products are cofunctional in many cells. Each gene appears to have a primary role during development, but also plays multiple roles in combination with other *Hox* genes. Further, the observed progression of both the *hoxd-3* and the *hoxa-3* mutant phenotypes as one or two copies of the paralogous genes are removed, argues that in normal animals, development is exquisitely sensitive to small changes in the concentration of their respective gene products. □

Received 18 April; accepted 24 June 1994.

1. Chisaka, O. & Capecchi, M. R. *Nature* **350,** 473–479 (1991).
2. Lufkin, T., Dierich, A., LeMeur, M., Mark, M. & Chambon, P. *Cell* **66,** 1105–1119 (1991).
3. Chisaka, O., Musci, T. S. & Capecchi, M. *Nature* **355,** 516–520 (1992).
4. LeMouellic, H., Lallemand, Y. & Brûlet, P. *Cell* **69,** 251–264 (1992).
5. Ramirez-Solis, R., Zheng, H., Whiting, J., Krumlauf, R. & Bradley, A. *Cell* **73,** 279–294 (1993).

6. Carpenter, E. M., Goddard, J. M., Chiska, O., Manley, N. R. & Capecchi, M. R. *Development* **118,** 1063–1075 (1993).
7. Mark, M. *et al. Development* **119,** 319–338 (1993).
8. Condie, B. G. & Capecchi, M. R. *Development* **119,** 579–595 (1993).
9. Jeannotte, L., Lemieux, M., Charron, J., Poirier, F. & Robertson, E. J. *Genes Dev.* **7,** 2085–2096 (1993).
10. Dollé, P. *et al. Cell* **75,** 431–441 (1993).
11. Small, K. M. & Potter, S. S. *Genes Dev.* **7,** 2318–2328 (1993).
12. Gendron-Maguire, M., Mallo, M., Zhang, M. & Gridley, T. *Cell* **75,** 1317–1331 (1993).
13. Rijli, F. M. *et al. Cell* **75,** 1333–1349 (1993).
14. Kostic, D. & Capecchi, M. R. *Mech. Dev.* (in the press).
15. Davis, A. P. & Capecchi, M. R. *Development* (in the press).
16. Hunt, P. *et al. Nature* **353,** 861–864 (1991).
17. McGinnis, W. & Krumlauf, R. *Cell* **68,** 283–302 (1992).
18. Aberdam, D., Negreanu, V., Sachs, L. & Blatt, C. *Molec. cell. Biol.* **11,** 554–557 (1991).
19. Dollé, P. *et al. Proc. natn. Acad. Sci. U.S.A.* **90,** 7666–7670 (1993).
20. Kessel, M. & Gruss, P. *Cell* **67,** 89–104 (1991).
21. Mansour, S. L., Goddard, J. M. & Capecchi, M. R. *Development* **117,** 13–28 (1993).
22. Jegalian, B. G. & DeRobertis, E. M. *Cell* **71,** 901–910 (1992).

ACKNOWLEDGEMENTS. We thank M. Allen, S. Barnett, J. Hayes, C. Lenz, E. Nakashima and S. Tamowski for technical assistance. L. Oswald helped with the preparation of the manuscript.

Cyclic ADP ribose activation of the ryanodine receptor is mediated by calmodulin

Hon Cheung Lee*, Robert Aarhus*, Richard Graeff*, Mary E. Gurnack† & Timothy F. Walseth†

Departments of * Physiology and † Pharmacology, University of Minnesota, Minneapolis, Minnesota 55455, USA

CYCLIC ADP-ribose (cADPR) is a newly identified nucleotide[1,2] which can release calcium from a variety of cells[3–6], suggesting it is a messenger for mobilizing internal Ca^{2+} stores. Its cyclic structure has now been confirmed by X-ray crystallography[7]. Available results are consistent with it being a modulator of Ca^{2+}-induced Ca^{2+} release[8–10]. Here we report that sea urchin egg microsomes purified by Percoll gradients lose sensitivity to cADPR, but the response can be restored by a soluble protein in the supernatant. Purification and characterization of the protein indicate that it is calmodulin. It appears to be sensitizing the Ca^{2+} release mechanism because caffeine and strontium, agonists of Ca^{2+}-induced Ca^{2+} release, can also mimic calmodulin in conferring cADPR-sensitivity. Although evidence indicates that cADPR may be an activator of the ryanodine receptor[8–10], present results point to the importance of accessory proteins such as calmodulin in modulating its activity.

During the initial investigations on the Ca^{2+}-mobilizing activities of cADPR, we noted the requirement of a soluble protein factor[1]. Sea urchin egg microsomes purified by Percoll density gradient centrifugation[1,11] lost the sensitivity to cADPR and did not release Ca^{2+} even when challenged by a saturating concentration of cADPR (Fig. 1*a*) The loss could be prevented by incubation with the supernatant obtained from the Percoll gradients. The concentration-dependency of preventing the loss of cADPR sensitivity by the supernatant is shown in the inset of Fig. 1*a*.

The cADPR-sensitivity-conferring factor is highly conserved because soluble extracts from dog brain can also substitute.

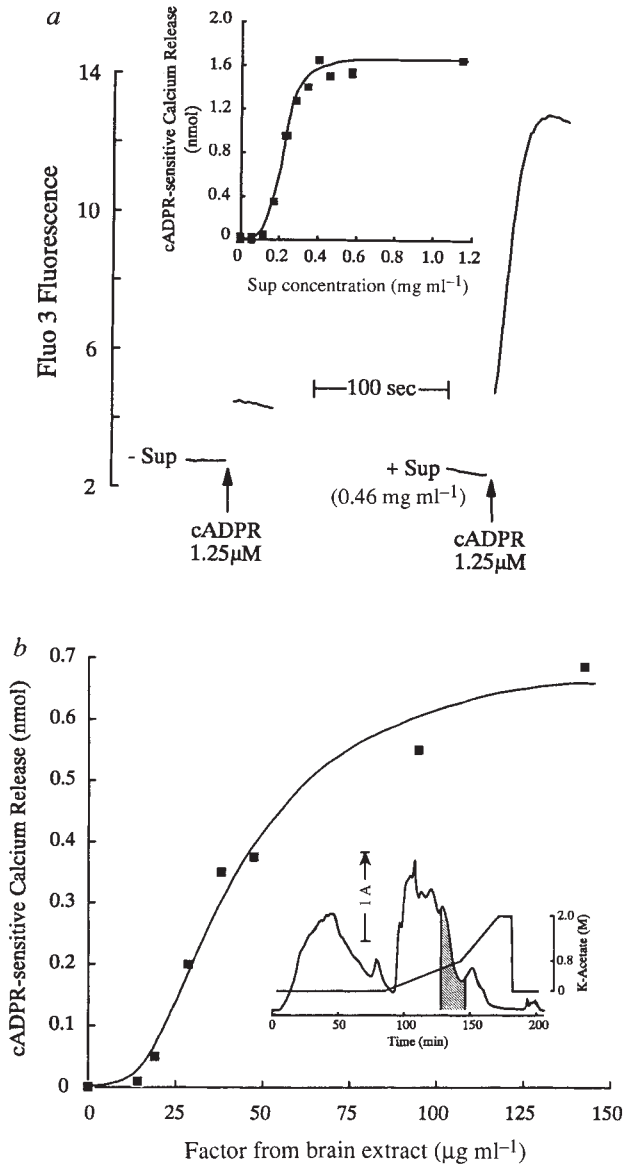

FIG. 1 Requirement of a soluble protein for cADPR-dependent Ca^{2+} release. *a*, Egg microsomes were incubated with (+Sup) or without (−Sup) the factor isolated from supernatants of egg homogenates. Ca^{2+} release was monitored by Fluo 3 (1–2 μM) and the fluorescence changes were calibrated by known amounts of Ca^{2+} as previously described[9]. The inset shows the concentration dependency of the soluble factor in reconstituting cADPR-sensitive Ca^{2+} release. *b*, A partially purified protein from brain can also confer cADPR sensitivity on egg microsomes in a concentration-dependent fashion. The inset shows fractionation of brain extracts on a DEAE 40 HR column. Elution was followed by absorbance at 280 nm (A). The cADPR-sensitivity-conferring activity of each fraction was assayed by incubating egg microsomes (0.4 ml) with various fractions (40 μl) for 2–3 h at 17 °C and then challenging with 1.25 μM cADPR. The shaded area in the elution profile (inset) indicates the active fractions that were used to construct the concentration–response curve.

METHODS. *S. purpuratus* eggs were homogenized by nitrogen decavitation and the microsomes purified by Percoll density centrifugation as previously described[11]. The soluble fraction (Sup) was prepared by centrifuging the Percoll supernatants at 227,000*g* for 30 min at 4°C. The microsomes were diluted 4–5-fold and incubated for about 3 h at 17 °C in a medium described previously[11]. The soluble extracts of frozen dog brains (Pel Freeze, Rogers, AR) were prepared by homogenization (25% w/v) in a buffer containing 0.34 M glucose, 1 mM $MgCl_2$ and 20 mM HEPES, pH 7.2, 10 μg ml^{-1} leupeptin, 10 μg ml^{-1} aprotinin and 50 μg ml^{-1} soybean trypsin inhibitor. Homogenization was first with a Tissumizer (Tecmar, OH) for 5 s and then 4 strokes with a Dounce glass homogenizer. The homogenates were centrifuged at 4 °C for 45 min at 300,000*g*. The supernatant (50 ml) was loaded onto a 25 × 95 mm DEAE 40 HR column (Waters, MA) and eluted with a potassium-acetate gradient prepared in 1 mM $MgCl_2$, 10 mM HEPES, pH 7.2, as shown in the inset of *b*. Active fractions were combined and further purified on a DEAE 5PW and a 300SW gel-filtration column (Waters). Starting with 333 mg soluble extract about 1.5 mg purified factor was obtained. The purification was 89-fold and the yield was 40%. The active factor in egg supernatants (Sup) was similarly purified on DEAE 5PW and 300SW gel-filtration columns.